Anisotropy of losses in grain-oriented Fe-Si

Anisotropy of losses in grain-oriented Fe–Si

Cite as: AIP Advances **11**, 115208 (2021); https://doi.org/10.1063/5.0066131
Submitted: 08 August 2021 • Accepted: 05 October 2021 • Published Online: 03 November 2021

E. Ferrara, C. Appino, C. Ragusa, et al.

Anisotropy of losses in grain-oriented Fe–Si

Cite as: AIP Advances 11, 115208 (2021); doi: 10.1063/5.0066131
Submitted: 8 August 2021 • Accepted: 5 October 2021 •
Published Online: 3 November 2021

View Online Export Citation CrossMark

E. Ferrara,[1] C. Appino,[1] C. Ragusa,[2,a)] O. de la Barrière,[3] and F. Fiorillo[1]

AFFILIATIONS

[1] Advanced Materials Metrology and Life Science Division, INRIM, 10135 Torino, Italy
[2] Department of Energy "Galileo Ferraris", Politecnico di Torino, 10129 Torino, Italy
[3] Lab. SATIE, CNRS/ENS Paris Saclay, 91190 Gif-sur-Yvette, France

[a)] **Author to whom correspondence should be addressed:** carlo.ragusa@polito.it

ABSTRACT

Comprehensive assessment of the magnetic behavior of grain-oriented steel (GO) Fe–Si sheets, going beyond the conventional characterization at power frequencies along the rolling direction (RD), can be the source of much needed information for the optimal design of transformers and efficient rotating machines. However, the quasi-monocrystal character of the material is conducive, besides an obviously strong anisotropic response, to a dependence of the measured properties on the sample geometry whenever the field is applied along a direction different from the rolling and the transverse (TD) directions. In this work, we show that the energy losses, measured from 1 to 300 Hz on GO sheets cut along directions ranging from 0° to 90° with respect to RD, can be interpreted in terms of linear composition of the same quantities measured along RD and TD. This feature, which applies to both the DC and AC properties, resides on the sample geometry-independent character of the RD and TD magnetization and on the loss separation principle. This amounts to state that, as substantiated by magneto-optical observations, the very same domain wall mechanisms making the magnetization to evolve in the RD and TD sheets, respectively, independently combine and operate in due proportions in all the other cases. By relying on these concepts, which overcome the limitations inherent to the semi-empirical models of the literature, we can consistently describe the magnetic losses as a function of cutting angle and stacking fashion of GO strips at different peak polarization levels and different frequencies.

I. INTRODUCTION

The role of grain-oriented (GO) steel sheets in the transmission and conversion of the electrical energy is increasingly challenged by novel applications, such as those enforced by the emerging "smart grid" technologies, the related medium-to-high frequencies conversion devices, and the development of efficient low-noise rotating machines.[1,2] Comprehensive knowledge of the material behavior, going beyond the usual assessment and implementation in the machine design of the properties measured along the rolling direction (RD), is therefore appreciated in the engineering practice. Besides the well-known example of large rotating machines,[3] recent advances have been made by the use of GO sheets in very-high-speed motors,[4] in turbogenerators,[5] and alone or in combination with non-oriented laminations, in switched reluctance motors,[6–8] showing reduced losses and noise. Small and medium power rotating machines with cores built of shifted non-segmented GO sheets are also shown to exhibit low reactive power and low loss.[9] Faced with these excellent perspectives in applications, the theoretical treatment of the magnetization process and losses and their evolution with the direction of the field in the lamination plane are typically limited to experiments made on conventional Epstein strips cut at different angles with respect to the Rolling Direction (RD).[10–14] For all their practical appeal and importance as a standard,[15] the Epstein frame measurements on strips cut at different angles θ to RD can only provide results belonging to such a specific sample geometry. The intrinsic response of the material, purged of the effect of the demagnetizing field at the strip edges, then becomes either difficult or impossible to experimentally retrieve by measurements, without resorting to cumbersome two-dimensional flux-closing structures. This is easily understood by looking at the GO strip as a good realization of a (110) [001] single crystal, where only with the [001] (RD) and $[1\bar{1}0]$ [Transverse Direction (TD)] cut strips we get rid of the lateral demagnetizing field $H_{d\perp}$. Even by resorting to circular samples and measuring the effective field by H-coils, we obtain that the magnetization curve at any defined angle θ to RD depends on the disk

diameter and thickness, according to the ratio between demagnetizing and coercive fields.[16] The demagnetizing field, non-collinear and in vector combination with the applied field, is the driving force for the dependence on the sample shape of the evolution of the 180° and 90° domain wall (dw) processes along the hysteresis loop at different θ values. Consequently, the usual experimental approach based on the Epstein frame or the single sheet/strip tester[17,18] can provide a range of results for identical θ and polarization values. The associated modeling of hysteresis and losses will therefore apply only for a particular measuring arrangement while relying on a number of adjustable parameters.[19] Such models often invoke energetic arguments, irrespective of the actual evolution of the domain structure and the related dw processes with θ.[10,20] On the other hand, the phenomenological approach based on the adaptation of Bunge's theory of the Orientation Distribution Function (ODF) to the prediction of the magnetic flux density for any angle θ through a cosine series and adjustable coefficients does not offer any connection with the underlying magnetization process.[13,14,21]

We can, however, obtain good information on the evolution of the domain structure along the hysteresis loop for different θ values and different sample shapes by magneto-optical imaging. Shin *et al.*[18] showed, by experiments on disk samples, that with the field applied along directions different from RD, the 180° [001] slab-like structure, filling the sample in the demagnetized state, is either partially or completely converted into [100] and [010] directed domains by 90° dw displacements under an increasing applied field. Such processes, eventually completed at high inductions by the rotation of the magnetization toward the field direction, cannot occur independent of the strength and direction of the demagnetizing field.

It was demonstrated in past work how the case of Epstein strips, tested using either a conventional frame or a single strip on a soft yoke, is quite an extreme one, where it is found that the magnetization is always constrained by the high lateral demagnetizing effect to lie along the applied (longitudinal) field direction, whatever the cutting angle θ.[22] The resulting internal field determines the fractional volumes occupied at any instant of time by the involved magnetic phases, the two main [001] phases, separated by the 180° dws, and the two [100] and [010] phases, the latter growing at the expense of the former by 90° dw motion upon leaving the demagnetized state. This results in near-zero magnetization transverse to the strip length, a condition progressively relaxed upon the increase of sample width. The magnetization process in the Epstein strips can therefore be *considered as having an intrinsic character only for* θ = 0° (*RD*) *and* θ = 90° (*TD*), a property seldom recognized in the literature. Of course, we do not need to have extremely wide sheet samples in order to neglect the demagnetizing field. It suffices to cross-stack the strips under test (provided they are not too narrow) in order to avoid flux leakage, as easily verified by the experiments, and recover the true $J(H)$ and loss behaviors. Figure 1 provides an illustrative example of the dramatic differences observed on the major quasi-static hysteresis loops and the energy losses measured in high-permeability (HGO) sheets cut at 75° and 45°, respectively, with respect to RD and tested as parallel-stacked Epstein strips (polarization aligned with the applied field) and cross-stacked (X-stacked) 120 mm wide strips (two-dimensional intrinsic response of the magnetization).

In this work, we present and discuss the results of an extensive investigation made on the loss behavior of parallel-stacked and X-stacked HGO Fe–Si sheet/strip samples as a function of the cutting angle θ. The experiments cover a range of peak polarization values (0.50 T ≤ J_p ≤ 1.40 T) and frequency f (1–300 Hz) and are supported by magneto-optical domain observations. It is shown that, whatever the case, it is possible to reconstruct to good

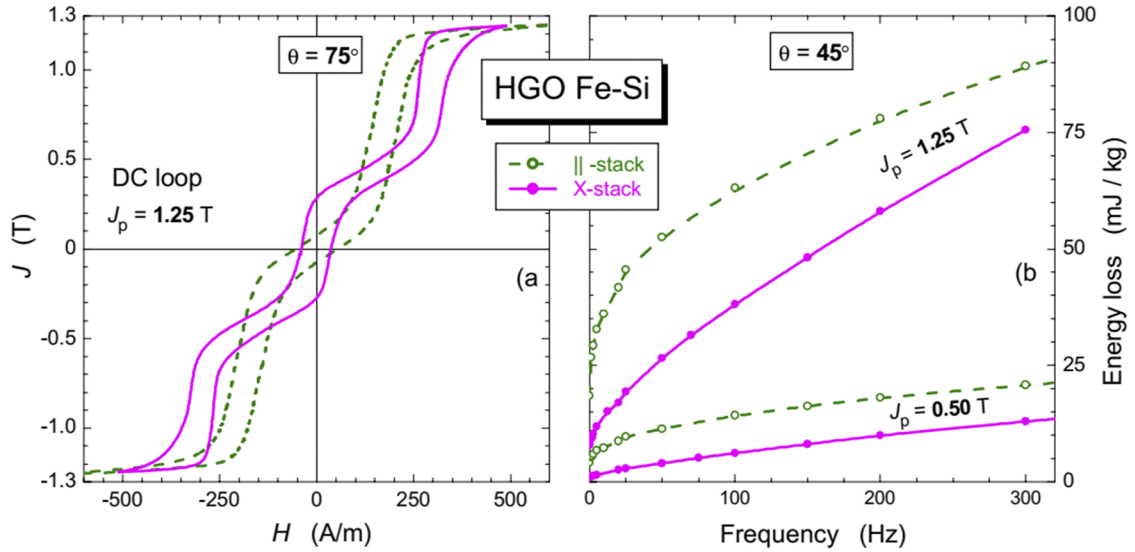

FIG. 1. (a) Quasi-static major hysteresis loops measured on parallel-stacked (||) Epstein strips and cross-stacked (X) HGO sheets cut at 75° to the rolling direction. (b) Energy loss vs frequency for different stacking modes and θ = 45° at two representative peak polarization values J_p. The large differences of magnetization curve and losses in the differently arranged strip samples reveal distinctive behaviors of the related dw processes.

approximation the measured losses by identification of the contributions provided by the domain wall processes separately operating in the [001] phases and the [100] and [010] ones. More precisely, we identify, for a generic angle θ, the contribution to the magnetization reversal provided by the 180° dw displacements, occurring within the [001] phases, and by the motion of the 90° dws, responsible for the growth/shrinkage of the [100] and [010] phases, in balance with the [001] ones. This amounts, in practice, to determine the loss components obtained by separate measurements on the RD and TD strips as a function of J_p and f and composing them, by virtue of their geometry-independent character, through a simple set of linear equations. These describe, for any θ, the volume balance of the different phases as a function of time. Although certain simplifications regarding the actual domain structure and its evolution with J_p, f, and θ are assumed in the model (e.g., single crystal approximation and absence of supplementary flux-closing domains), the identified magnetization mechanisms are shown to provide quantitative interpretation of the anisotropic behavior of the material.

II. MAGNETIZATION PROCESS VS ANGLE TO RD

A. Domains and magnetic phases

Magneto-optical imaging is usefully performed in HGO Fe–Si sheets by taking advantage of a relatively simple domain structure.[23] It permits one, in particular, to draw a relationship between the magnetization curve and the cutting angle θ in terms of specific domain wall processes. Shin *et al.*[18] confirmed by observations on circular samples that, with the field applied along TD, the magnetization proceeds through progressive transformation by 90° dw motion of the [001] phases, filling the sample volume in the demagnetized state, into the [100] [010] phases, equally sharing their contributions and eventually covering the whole sample at the polarization value $J_p = J_s/\sqrt{2}$. Magnetostrictive requirements can produce changes in the topology of these two phases under increasing (or decreasing) field strength, as signaled by changes of orientation and spacing of the flux-closing surface domain patterns.[18] When the same observations are made on the HGO strips cut along a generic angle θ, it is concluded that both 180° dw motion in the [001] phases and the [001] → [100] [010] transition mechanism, guided by 90° dw displacements, can occur. These processes balance not only according to the specific θ value but also on aspect ratio and stacking mode of the strip samples. Figure 2 compares the major hysteresis loops of 45°-cut parallel-stacked and X-stacked strips with correspondingly taken frames of the domain structure. The dramatic difference of the magnetization curves finds its rationale in the conspicuously different evolution of the domain structure.[22] For example, with the vanishing demagnetizing field at the strip edges and $\theta < 54.7°$, the [001] phases alone can cope with the longitudinally applied field $\boldsymbol{H}$ in the X-stacked samples. The measured hysteresis loop at the peak polarization J_p will then simply coincide with the projection along $\boldsymbol{H}$ of the RD loop of amplitude $\pm J_p/\cos 45°$. Once

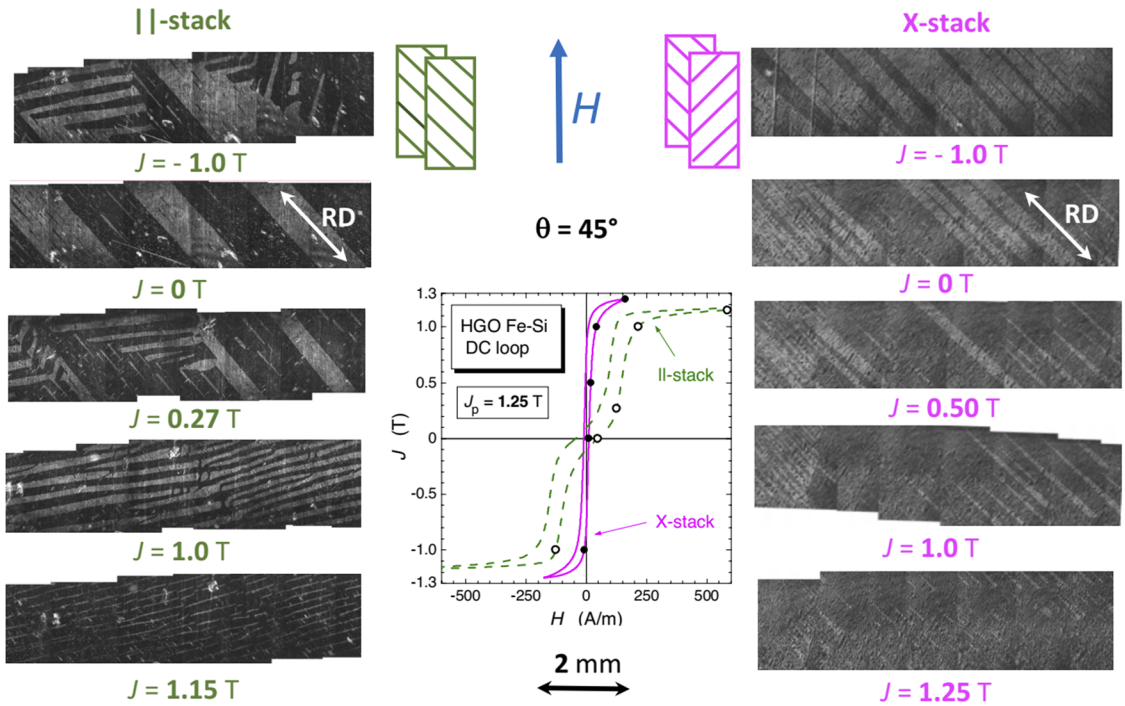

FIG. 2. Evolution of the domain structure along the ascending branch of a major hysteresis loop (J_p = 1.25 T) in parallel-stacked (left column) and X-stacked (right column) HGO Epstein strips cut at 45° with respect to RD. When moving away from the demagnetized state, fully occupied by the [001] phases, the [100] and [010] phases emerge and grow by the motion of 90° dws in the parallel-stacked strips, as signaled by the appearance and growth of the flux-closing surface structures. The [100] phases persist instead along the whole cycle in the X-stacked strips. A clear correlation can be established between these processes and the hysteresis loop behaviors.

saturated (*end of Néel's Mode I*), the [001] phase will respond to the increasing $\boldsymbol{H}$ value by coherent rotation of the magnetization (*Mode IV*).

The domain structures and processes underlying the conventional measurements on parallel-stacked Epstein strips are sketched in Fig. 2(a). It appears that on leaving the demagnetized state and its regular antiparallel [001] domain pattern, the [100] and [010] phases start to participate in the magnetization reversal, as signaled by the appearance of the flux-closing domains. It is indeed realized that because of the high aspect ratio of the strip and the correspondingly strong lateral demagnetizing effect, the different phases balance their contributions by motion of the 180° and 90° dws in such a way to make the transverse magnetization negligible. By virtue of this condition, the balanced dw processes will end, under increasing applied field, upon achieving the so-called Kaya's condition, where three phases survive and the polarization becomes

$$J_K = \frac{J_s}{l+m+n}, \tag{1}$$

where J_s is the saturation polarization and l, m, and n are the direction cosines made by $\boldsymbol{H}$ with the easy axes. For symmetry reasons, the internal field $\boldsymbol{H}_i$ points along the [111] direction and the magnetization rotates in all the three phases (*Mode II*) until the approach to saturation.

The rotation regime can be subjected, through energy minimization, to defined analytical description.[22] One cannot do the same, in general, to describe the complexity of the dw processes. However, we can exploit the intrinsic (geometry independent) character of the loss behavior of the RD and TD strip samples and take the related figures as building blocks of the quasi-static and dynamic response of the material, in particular, the parallel-stacked and X-stacked strips, for any angle θ. This amounts to assuming that the very same physical mechanisms, independently operating in the RD and TD strips, share in suitable proportions the reversal of the magnetization along all the other directions in the sheet plane. We obviously offer in this way a simplified view of the actual magnetization process by assimilating the HGO samples to perfectly oriented (110)[001] single crystals and independently treating what could be interacting processes when θ is different from 0° to 90°. The question is therefore posed regarding the degree of accuracy by which we can describe the anisotropy of losses from knowledge of the material behavior along RD and TD. An example, regarding the energy loss vs frequency $W(f)$ and the quasi-static hysteresis loop, is anticipated in Fig. 3.

B. The RD and TD processes combine to provide the magnetization reversals in any direction

The magnetization process in the plane of the HGO sheets occurs, in the most general case, through the evolution of the two [001] phases by 180° dw displacements and by the concurrent balanced growth/decrease of the [100] [010] phases by the motion of the 90° dws. This is what is induced by the Kerr observation of the domain structure and the evolution of the hysteresis loop shape vs θ (see Figs. 2 and 3 and the supplementary material).

Let us define the fractional sample volume occupied at any instant of time by the [001] phase as v_{180} and the remainder, occupied by the [100] and [010] phases, symmetrically directed with respect to the sheet plane, as v_{90}. It is $v_{180} + v_{90} = 1$, and as a limit, $v_{180} = 1$ both in the RD strips and in the demagnetized TD strips. In the latter, we eventually attain $v_{90} = 1$ for $J = J_s/\sqrt{2}$. With reference to Fig. 4, we state that, on attaining the longitudinal polarization value

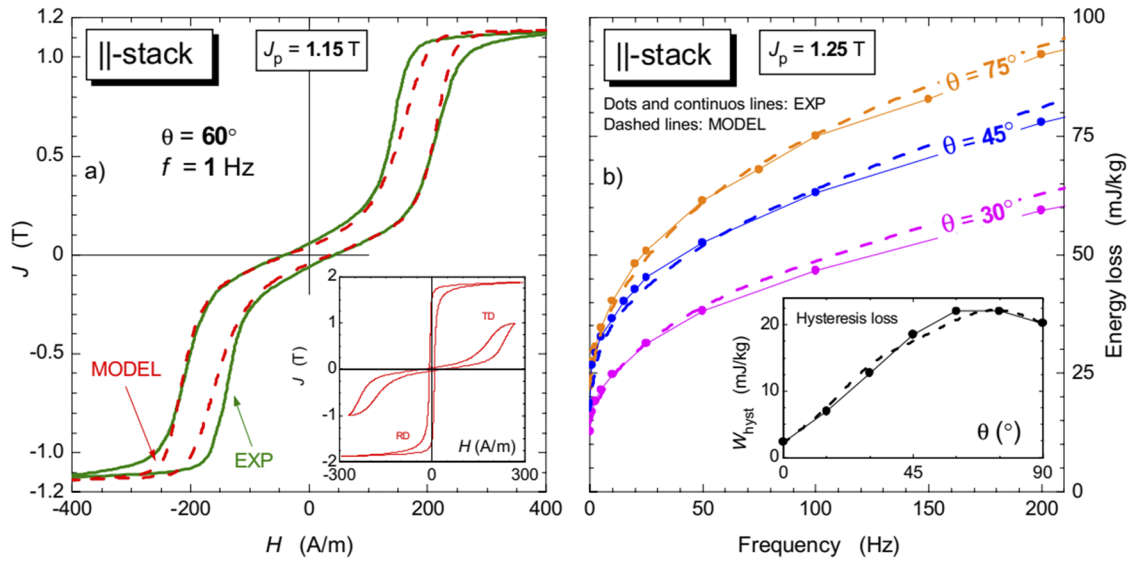

FIG. 3. Example of measured and predicted hysteresis loop and energy loss $W(f)$ behaviors in parallel-stacked GO Epstein strips (thickness 0.289 mm) cut at an angle θ to RD. The dependence of the quasi-static loss W_{hyst} is separately shown in the inset of (b). The quasi-static hysteresis loop in (a) is modeled (dashed line) by the volume-weighted composition of the RD and TD quasi-static loops shown in the inset.

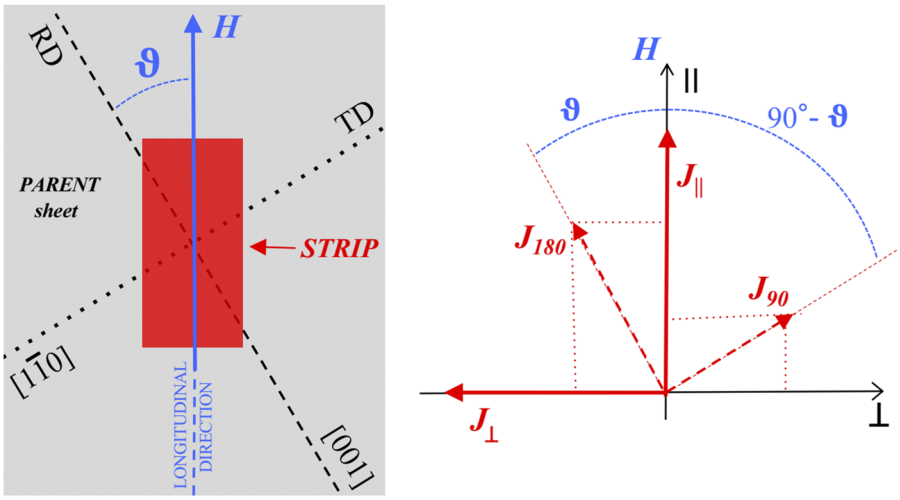

FIG. 4. The measured strips are cut out of the parent GO sheet along a direction making an angle θ with respect to the Rolling Direction (RD). With a longitudinally applied field ***H***, the magnetization variation is shared by three easy directions (magnetic phases), and both longitudinal $J_{||}$ and transverse $J_{\perp}$ components in the sheet plane are measured. $J_{||}$ and $J_{\perp}$ result from the displacements of 180° dws in the [001] phases (J_{180}) and the growth/decrease in the [100] [010] phases, in balance with the [001] ones, by 90° dw transitions (J_{90}). The evolution of these contributions under a changing applied field is described by Eqs. (3) and (4).

$J_{||}$ on the strip cut at the angle θ, the [001] phases reach, inside their volume v_{180}, the level $J_{180}^{(r)}$. We write the related contribution to $J_{||}$, averaged over the whole sample volume, as

$$J_{180}\cos\theta = J_{180}^{(r)} v_{180}\cos\theta. \tag{2}$$

It is easily realized that the polarization inside v_{90}, pointing along the direction $(\pi/2 - \theta)$ in the sheet plane, is always $J_{90}^{(r)} = J_s/\sqrt{2}$, and its contribution to $J_{||}$ is $J_{90}\sin\theta$, with $J_{90} = v_{90}\cdot J_{90}^{(r)}$. We thus write the longitudinal (applied field directed) $J_{||}$ and the transverse $J_{\perp}$ polarization values as

$$J_{||} = J_{180}\cos\theta + J_{90}\sin\theta, \tag{3}$$

$$J_{\perp} = J_{180}\sin\theta - J_{90}\cos\theta. \tag{4}$$

Equations (3) and (4) apply at all frequencies whatever the strip width. Determination of $J_{||}(t)$ and $J_{\perp}(t)$ is thus all we need to retrieve the loss contributions by the RD and TD processes. These

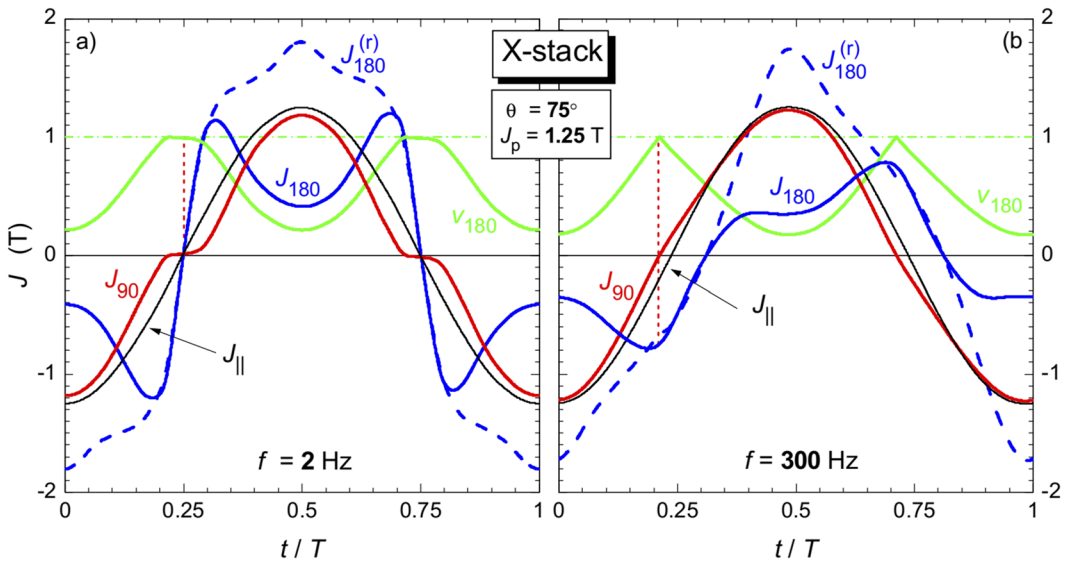

FIG. 5. X-stacked strips cut at $\theta = 75°$ are tested at 2 (a) and 300 Hz (b) ($T = 1/f$) under sinusoidal polarization $J_{||}(t)$ at peak value $J_p = 1.25$ T. The individual strips are endowed with measurable transverse magnetization $J_{\perp}(t)$, whose behavior permits one to obtain, via Eqs. (3)–(5), the contributions $J_{180}(t)$ and $J_{90}(t)$ provided by the [001] and [100] [010] phases, respectively, besides their fractional volumes $v_{180}(t)$ and $v_{90}(t)$ ($v_{180}(t) + v_{90}(t) = 1$). The quantity $J_{180}^{(r)}(t) = J_{180}(t)/v_{180}(t)$ is the polarization value referred to $v_{180}(t)$. Eddy current fields modify, for a same $J_{||}(t)$, the relative contribution, phase relationship, and degree of distortion of $J_{180}(t)$ (RD) and $J_{90}(t)$ (TD).

are assumed to linearly combine, thereby providing the energy loss $W(f, \theta)$ at any peak polarization value lower than J_K [as defined in Eq. (1)]. For $J_{||} > J_K$, the rotational processes are predicted by the approach discussed in Ref. 22. Once the quantities $J_{180}(t)$ and $J_{90}(t)$ are calculated from the measured $J_{||}$ and $J_{\perp}$ by means of Eqs. (3) and (4), the fractional volumes

$$v_{90}(t) = J_{90}(t) \cdot \frac{\sqrt{2}}{J_s} \tag{5}$$

and $v_{180}(t) = 1 - v_{90}(t)$ and the reduced polarization

$$J_{180}^{(r)}(t) = \frac{J_{180}(t)}{v_{180}(t)} \tag{6}$$

are obtained.

We are interested in the response of the material tested under sinusoidal $J_{||}(t)$ waveform and its relationship with the geometry-independent properties measured along RD ([001]) and TD ([1$\bar{1}$0]). We connect in this way little assessed properties of practical materials to the old fundamental questions related to the characterization of iron single crystals in different directions.[24] Figure 5 shows the representative case of X-stacked strips, cut at 75° to RD, measured both under quasi-static conditions and at 300 Hz. By this arrangement, the flux is fully closed, the lateral demagnetizing field is eliminated, and the observed properties have intrinsic character. To note that the imposed sinusoidal $J_{||}(t)$ (peak value J_p = 1.25 T) is decomposed into the non-sinusoidal waveforms $J_{180}(t)$ ([001]) and $J_{90}(t)$ ([100] [010]), as calculated through Eqs. (3) and (4) from the measured $J_{||}(t)$ and $J_{\perp}(t)$. In the absence of the demagnetizing field, the evolution of the magnetization process vs frequency is regulated by the balanced pressures of the applied field and the resisting coercive and eddy current fields. The role of the coercive field (not envisaged in the phase theory) is recognized in the time dependence of $J_{180}(t)$, $J_{90}(t)$, and $v_{180}(t)$ observed across the period $T = 1/f$ in

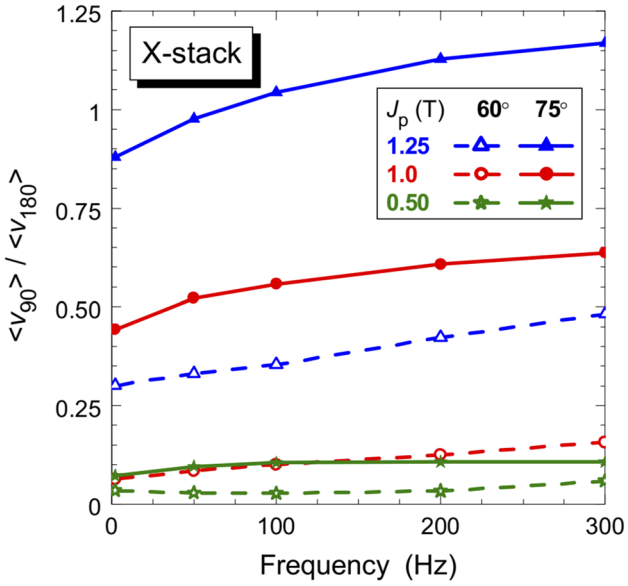

FIG. 6. The period-averaged fractional sample volume $\langle v_{90} \rangle$ ([100] and [010] phases) increases with frequency, for a given J_p, at the expense of $\langle v_{180} \rangle$ ([001] phases). In fact, the eddy currents restrain more effectively the motion of the 180° dws with respect to the 90° dw transitions.

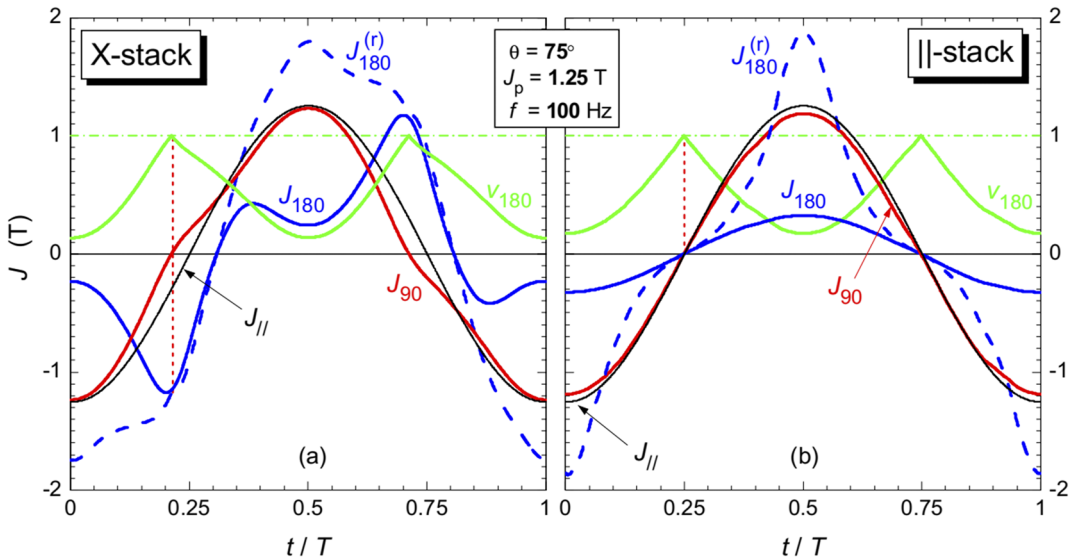

FIG. 7. The parameters involved in the magnetization process at 100 Hz and J_p = 1.25 T are compared for the X-stacked (a) and parallel-stacked 75°-cut strips (b). The behavior of the latter is overwhelmingly affected by the lateral demagnetizing field, which imposes not only equal and opposite transverse components $J_{180}(t) \cdot \sin\theta$ and $J_{90}(t) \cdot \cos\theta$, but also, in general, frequency-independent sharing of the magnetization process by the involved magnetic phases. Note that $J_{180}(t)$ and $J_{90}(t)$ in (b) attain zero value for v_{180} = 1, which is not the case for the X-stacked strips.

the X-stacked sheets under quasi-static excitation [see Fig. 5(a) for $\theta = 75°$]. One can see how the harder [100] [010] phases [$J_{90}(t)$] are stuck around the demagnetized state at time $t = 0.25T$, while most of the softer [001] dw displacements [$J_{180}(t)$] concurrently occur and $\nu_{180} \sim 1$. Eddy currents impose, however, an obvious change in the relative proportions of $J_{180}(t)$ and $J_{90}(t)$ and their phase relationship with increasing frequency, as demonstrated by the evolution of these quantities on passing from 2 to 300 Hz in Fig. 5(b). Figure 6 shows how the average value $\langle \nu_{90} \rangle$ correspondingly increases at the expense of $\langle \nu_{180} \rangle$ at all inductions. This occurs because the macroscopic (classical) eddy current patterns, whose counterfield equally acts on all the participating phases, impose greater restraint on the motion of the softer 180° dws.

Because of the non-identical frequency dependence of the 180° and 90° dw processes, the simultaneous knowledge of $J_{||}(t)$ and $J_{\perp}(t)$ is generally required for a full description of magnetic losses, while Eqs. (2)–(6) retain their validity whatever the strip width and stacking mode. Remarkably, however, the standard condition of parallel-stacked Epstein strips (and, *a fortiori*, of narrower strips) brings about, in force of the high lateral demagnetizing effect, the condition $J_{\perp}(t) = 0$ in Eqs. (3) and (4). The sole conventional measurement of $J_{||}(t)$ suffices in this case for achieving a full analysis of quasi-static and dynamic losses based on the knowledge of the RD and TD properties. It is an important simplification of the problem, which is expected to apply in many practical circumstances, like the ones met in GO-built rotating machine cores. The analysis of the parameters correspondingly involved in the composition of the RD and TD quantities, carried out by Eqs. (2)–(6), shows that $J_{180}(t)$ and $J_{90}(t)$ are sinusoidal and in phase with $J_{||}(t)$ [see Fig. 7(b)], whatever the frequency and the J_p value. Their relative proportions are indeed frozen-in by the demagnetizing field $H_{d\perp}$, overriding the effect on $J_{\perp}(t)$ by the eddy current field. It is then observed in the example of Fig. 7 that the very same measured sinusoidal $J_{||}(t)$ of peak value $J_p = 1.25$ T at 100 Hz results from the combination of very different $J_{180}(t)$ and $J_{90}(t)$ components in the X-stacked and parallel-stacked strips.

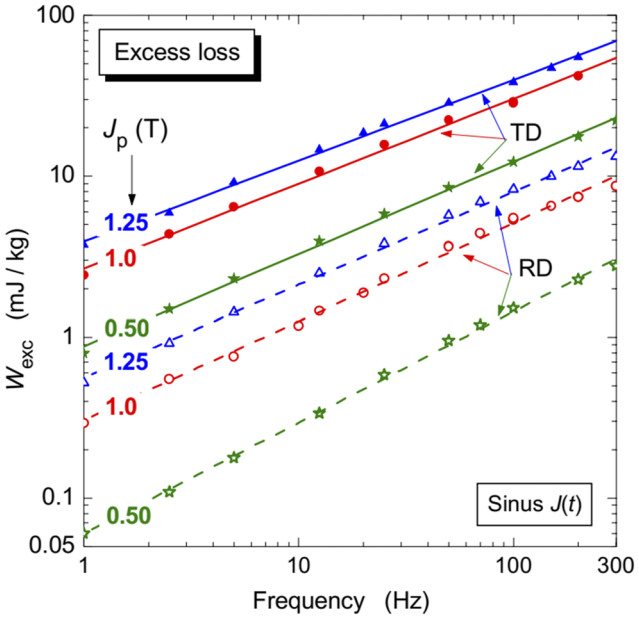

FIG. 9. The dependence of the excess loss on frequency follows to good approximation a power law. This figure shows the behavior of $W_{exc}(f)$ observed in the RD and TD strips at three different J_p values, from which we obtain that $W_{exc}(f) \propto f^{0.45-0.67}$.

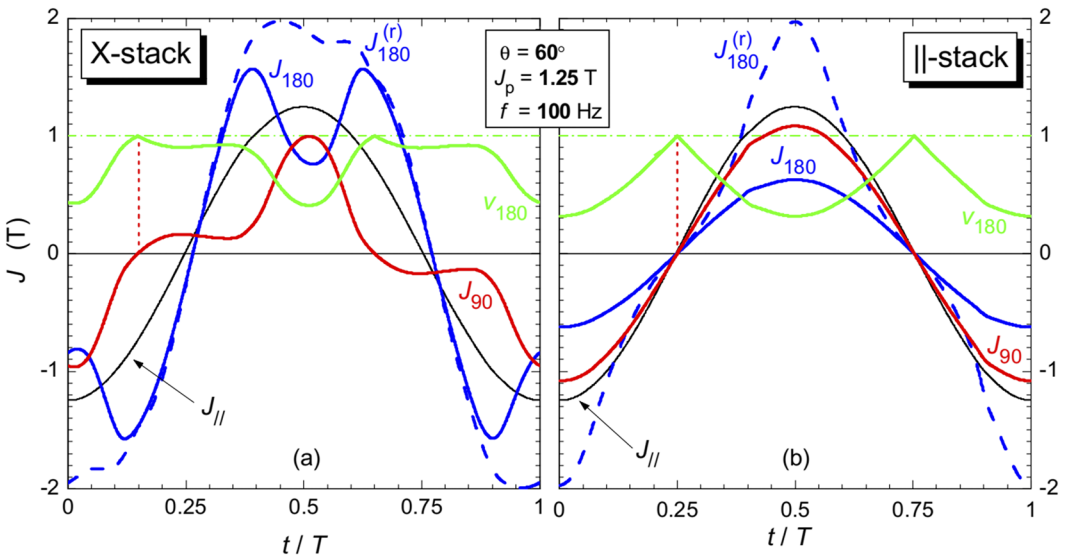

FIG. 8. Same as Fig. 7 for $\theta = 60°$. Note in (a) the large delay of $J_{180}(t)$ [i.e., $J_{180}^{(r)}(t)$] with respect to $J_{90}(t)$ on the return from peak induction. In the absence of $H_{d\perp}$, the magnetostrictive pressure is responsible for anticipated drop of J_{90} upon release of the applied field. The same $H_{d\perp}$ field drives instead $J_{180}(t)$ and $J_{90}(t)$ through regular in-phase sinusoidal behavior for parallel stacking (b).

III. ENERGY LOSS VS θ, J_p, f, AND STACKING MODE: EXPERIMENTAL AND DISCUSSION

A. Experimental method

High-permeability HGO sheets (M2H-type, thickness 0.289 mm) were cut by guillotine punching along directions ranging from RD to TD at 15° intervals. 300 × 30 mm^2 strips were tested, from 1 to 300 Hz, using both a conventional Epstein frame and a reduced Single Sheet Tester (SST), obtained as a double-C 300 mm long laminated yoke with 140 × 30 mm^2 plane pole faces. A 288-turn flat solenoid, incorporating a 250-turn secondary winding, was used as a primary of the SST. The magnetic path length was correspondingly defined, for any angle θ, as the one providing the same loss figure of the Epstein frame at 50 Hz, with three strips placed side by side at a distance of 15 mm. The same SST was also used to test 120 mm wide strip samples as cross-stacked pairs. A supplementary few-turn longitudinal winding, made with a 0.1 mm diameter wire, was used to detect the transverse magnetization $J_\perp$.

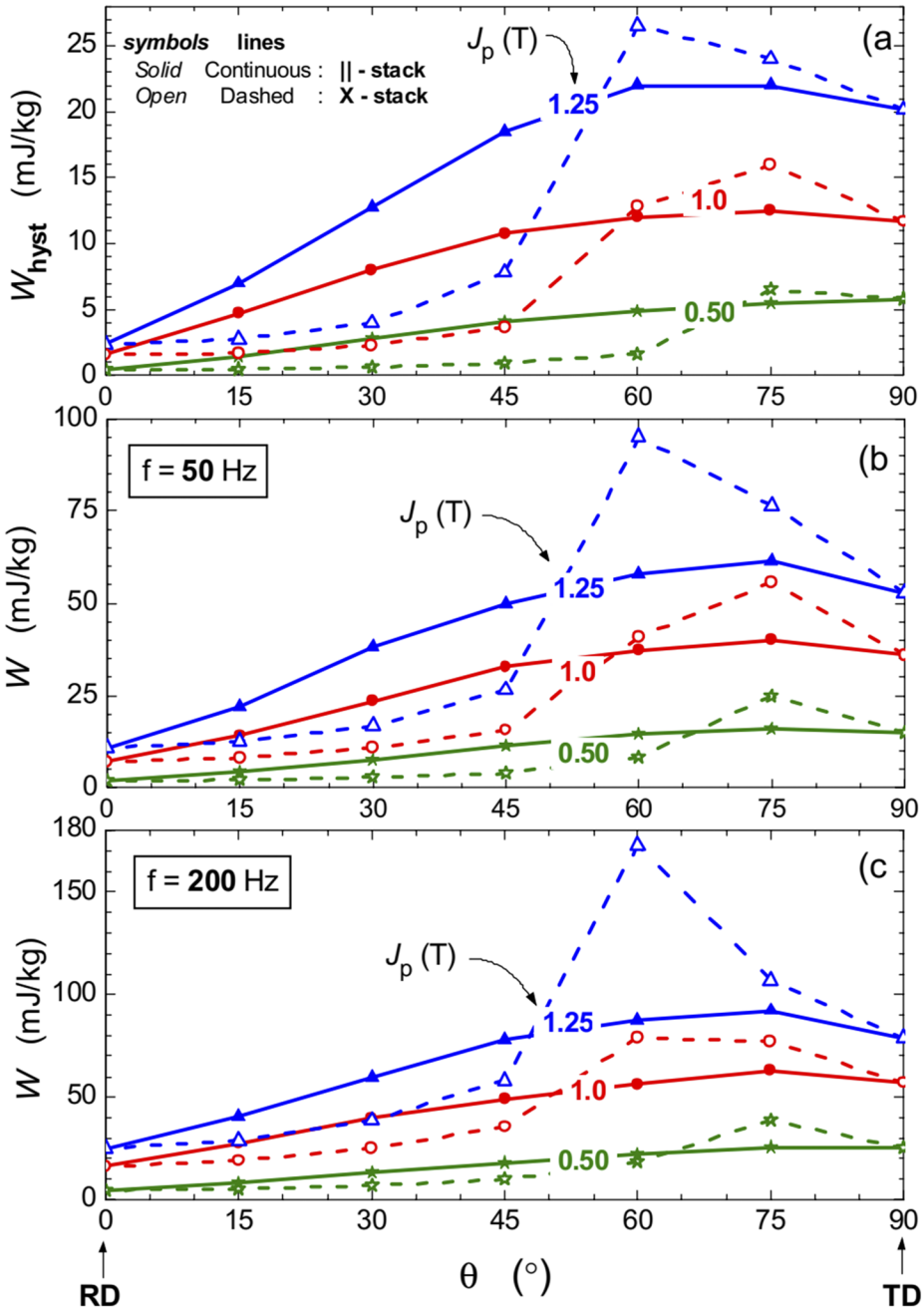

FIG. 10. The quasi-static (a) and dynamic [50 (b) and 200 Hz (c)] energy losses measured in the parallel-stacked and X-stacked strips are shown as a function of the cutting angle θ for three different values of the peak polarization. The more or less regular behavior of $W(\theta)$ in the parallel-stacked samples contrasts with a sharp increase in the X-stacked strips at large angles. The intrinsic response of the material, as achieved by cross-stacking, is fully accomplished by 180° dw motion of the [001] phases for $\theta < 54.7°$ ([111] directed sheet cutting). It involves the additional evolution of the harder [100] [010] phases at larger θ values.

It is observed that $J_\perp \sim 0$ in both parallel-stacked strips and X-stacked pairs. This demonstrates, on the one hand, the role of the demagnetizing field $H_{d\perp}$ in suppressing $J_\perp$ in relatively narrow strips and, on the other hand, the excellent flux closure obtained in the cross-stacked pairs. The latter finding implies that, at any instant of time, the polarization of the material $\boldsymbol{J}(t) = \boldsymbol{J}_{||}(t) + \boldsymbol{J}_\perp(t)$ inside the individual X-stacked strips is to very good approximation the one we would expect for an infinitely extended sheet (obviously averaged over a suitably wide area).

The characterization was performed, across the whole frequency range, under controlled sinusoidal $J_{||}(t)$ by means of a digital hysteresis graph-wattmeter, according to the well-assessed methodology.[25] The DC (quasi-static) energy loss W_{hyst} was obtained, according to the loss decomposition principle,[26] by subtracting the classical loss component $W_{class}(f)$ to the measured loss $W(f)$ and extrapolating the remaining quantity, $W_{hyst} + W_{exc}(f)$, the sum of quasi-static and excess losses, to $f \to 0$. The testing of the X-stacked strips was made by associating the measurement of $J_{||}(t)$ on the pair with the simultaneous measurement of $J_\perp(t)$ in the individual strips. The signal acquisition, amplification, and conversion was made by means of low-noise SRS 560 amplifiers and a four-channel 12 bit 500 MHz LeCroy oscilloscope working in a VEE environment.

B. The loss results and their interpretation

The interpretation of the quasi-static and dynamic energy losses in the GO sheets and their dependence on angle θ and sample geometry starts from the determination of the $J_{180}(t)$ and $J_{90}(t)$ behaviors, like the ones observed in Figs. 5, 7, and 8, and their assumed relationship with the known behavior of the losses in the RD and TD strips. With parallel-stacked Epstein strips, $J_\perp = 0$, and for imposed longitudinal polarization $J_{||}(t)$, we have

$$J_{180}(t) = J_{\parallel}(t)\cos\theta, \quad J_{90}(t) = J_{\parallel}(t)\sin\theta. \tag{7}$$

By Eq. (5), we calculate the fractional volume $v_{90}(t)$ occupied by the [100] [010] phases and the [001] fractional volume $v_{180}(t) = 1 - v_{90}(t)$. With large and X-stacked strips, exhibiting either partial or full closure of the lateral flux, $J_\perp \neq 0$ and from its measurement, we obtain, via Eq. (2),

$$J_{180}(t) = J_{\parallel}(t)\cos\theta + J_\perp(t)\sin\theta, \; J_{90}(t) = J_{\parallel}(t)\sin\theta - J_\perp(t)\cos\theta, \tag{8}$$

with $v_{90}(t)$ and $v_{180}(t)$ evolving as illustrated in the examples of Figs. 5, 7, and 8.

Whatever the case, once the time dependence of $J_{180}(t)$ and $J_{90}(t)$ over a period T is known, we easily arrive at the calculation of the energy loss $W(J_p, \theta, f)$ by resorting to the loss figures belonging to the RD and TD strips and their decomposition into the hysteresis W_{hyst}, classical W_{class}, and excess W_{exc} components. Let us then assume that, for defined θ and J_p values, we get, as previously described, $J_{180}(t)$, $J_{90}(t)$, and $v_{180}(t)$. The reduced polarization $J^{(r)}_{180}(t)$ is obtained from Eq. (6), and the loss components, taking into account the volumetric proportions of the involved magnetic phases, are calculated. The examples shown in Figs. 5, 7, and 8 show that $J_{90}(t)$ and $J^{(r)}_{180}(t)$ can be affected by distortion, with ensuing effects on W_{class}, and W_{exc}.

We start by writing the hysteresis loss as

$$W_{hyst}(J_p, \theta) = W_{hyst}\left(J^{(r)}_{180,p}\right)\langle v_{180}\rangle + W_{hyst}(J_{90,p}), \tag{9}$$

the weighted combination of W_{hyst} measured on the RD and TD strips at peak polarizations $J^{(r)}_{180,p}$ and $J_{90,p}$, respectively. $\langle v_{180}\rangle$ is the

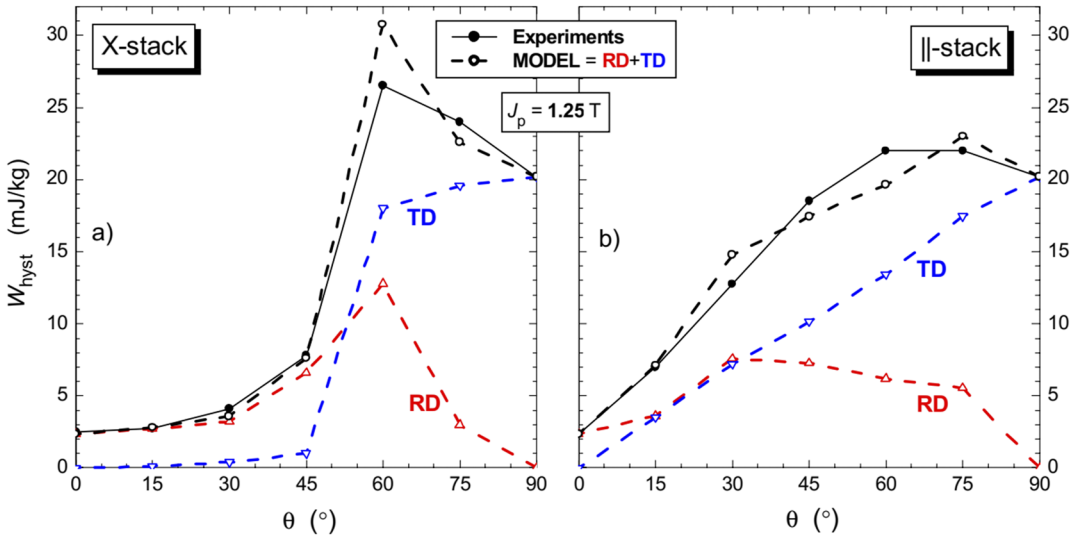

FIG. 11. Quasi-static energy loss vs θ in X-stacked (a) and parallel-stacked (b) strips for J_p = 1.25 T and calculated contributions by the [001] (180° dws), RD and [100] [010] (90° dws), TD phases $W_{hyst}(J_p) = W_{hyst}\left(J^{(r)}_{180,p}\right)\langle v_{180}\rangle + W_{hyst}\left(J_{90,p}\right)$.

period-averaged fractional volume of the [001] phase. The classical loss is calculated at any frequency f as

$$W_{\text{class}}(J_p, \theta, f) = \frac{\sigma d^2}{12\delta} \cdot \left(\langle v_{180} \rangle \int_0^T \left(\frac{dJ_{180}^{(r)}}{dt} \right)^2 dt + \int_0^T \left(\frac{dJ_{90}}{dt} \right)^2 dt \right) \quad \text{(J/kg)}, \qquad (10)$$

where σ and δ are the material conductivity and density, respectively. With this formulation, we take into account the actual non-sinusoidal behavior of $J_{180}^{(r)}(t)$ and $J_{90}(t)$.[27] The same is done for the excess loss $W_{\text{exc}}(J_p, \theta, f)$, following the framework offered by the Statistical Theory of Losses (STLs).[26,28] By this theory, we can express $W_{\text{exc}}(f)$ under generic induction waveform in terms of the same quantity measured under sinusoidal induction.[27] More specifically, we write

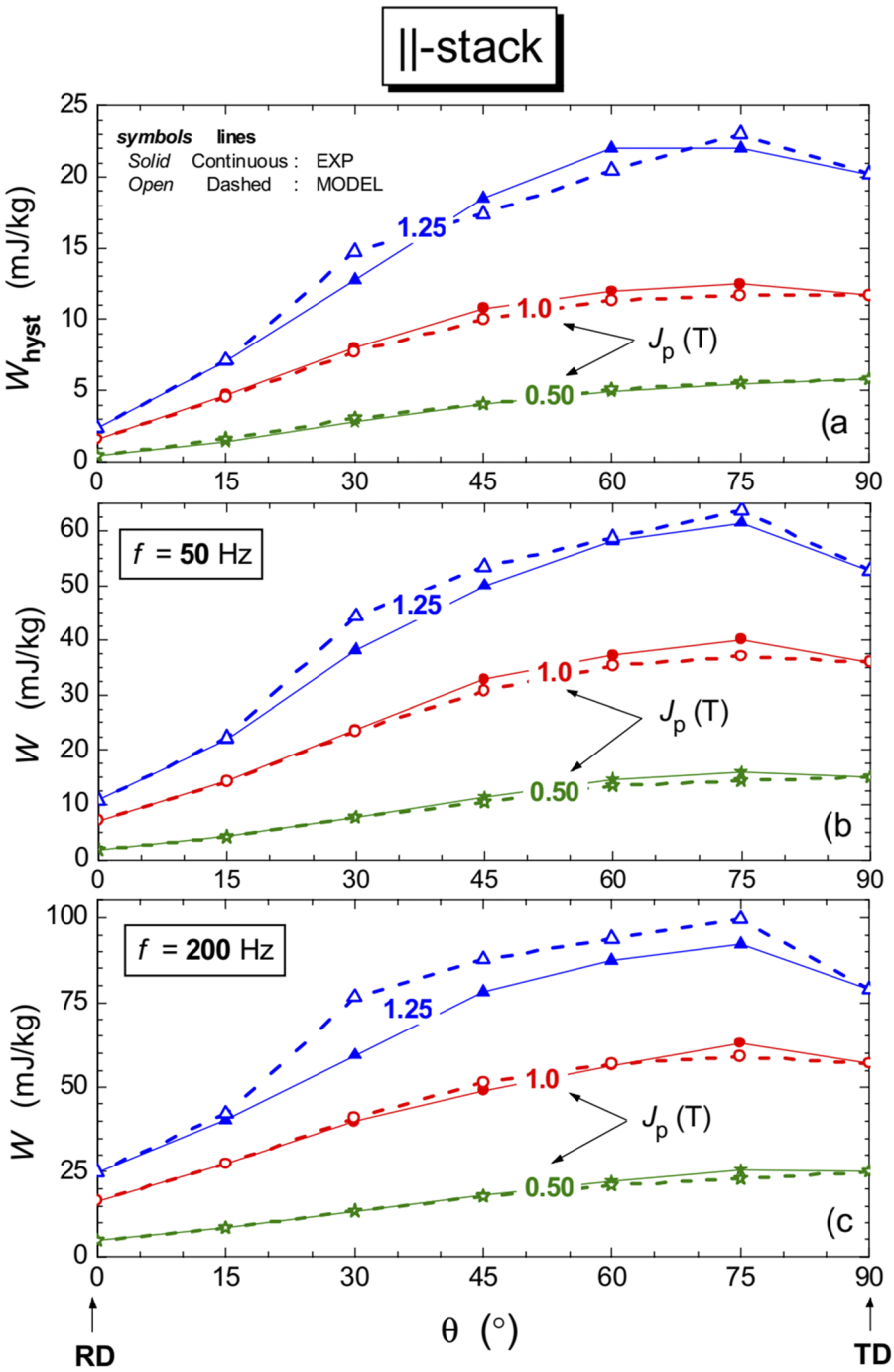

FIG. 12. Experimental vs modeled energy loss dependence on the cutting angle θ in parallel-stacked Epstein strips. Besides the quasi-static loss W_{hyst} (a), the measured and predicted loss figures at 50 (b) and 200 Hz (c) are considered for three different J_p values. The calculations are made according to Eqs. (9)–(15).

$$W_{\mathrm{exc}}(f) \propto \int_0^T |dJ/dt|^n \mathrm{d}t, \tag{11}$$

where, in general, $n = 3/2$ in magnetic steels. In the GO sheets magnetized along RD or TD, the results agree with n ranging between 1.67 and 1.45 on increasing J_p from 0.50 to 1.40 T. This results in a power law dependence on frequency $W_{\mathrm{exc}}(f) \propto f^{\,n-1}$, as illustrated in the example shown in Fig. 9, and it permits one to express the excess loss contributed by the non-sinusoidal polarization components $J_{180}^{(r)}(t)$ and $J_{90}(t)$ through the value of their sinusoidal counterparts $W_{\mathrm{exc,SIN}}(f)$, according to the equations

$$W_{\mathrm{exc}}\left(J_{180,\mathrm{p}}^{(r)}, f\right) = \langle v_{180}\rangle W_{\mathrm{exc,SIN}}\left(J_{180,\mathrm{p}}^{(r)}, f\right) \times \frac{\int_0^T \left|\mathrm{d}J_{180}^{(r)}/\mathrm{d}t\right|^n}{J_{180,\mathrm{p}}^{(r)\,\frac{3}{2}}(2\pi f)^{1/2}\int_0^{2\pi}|\cos\alpha|^n d\alpha}, \tag{12}$$

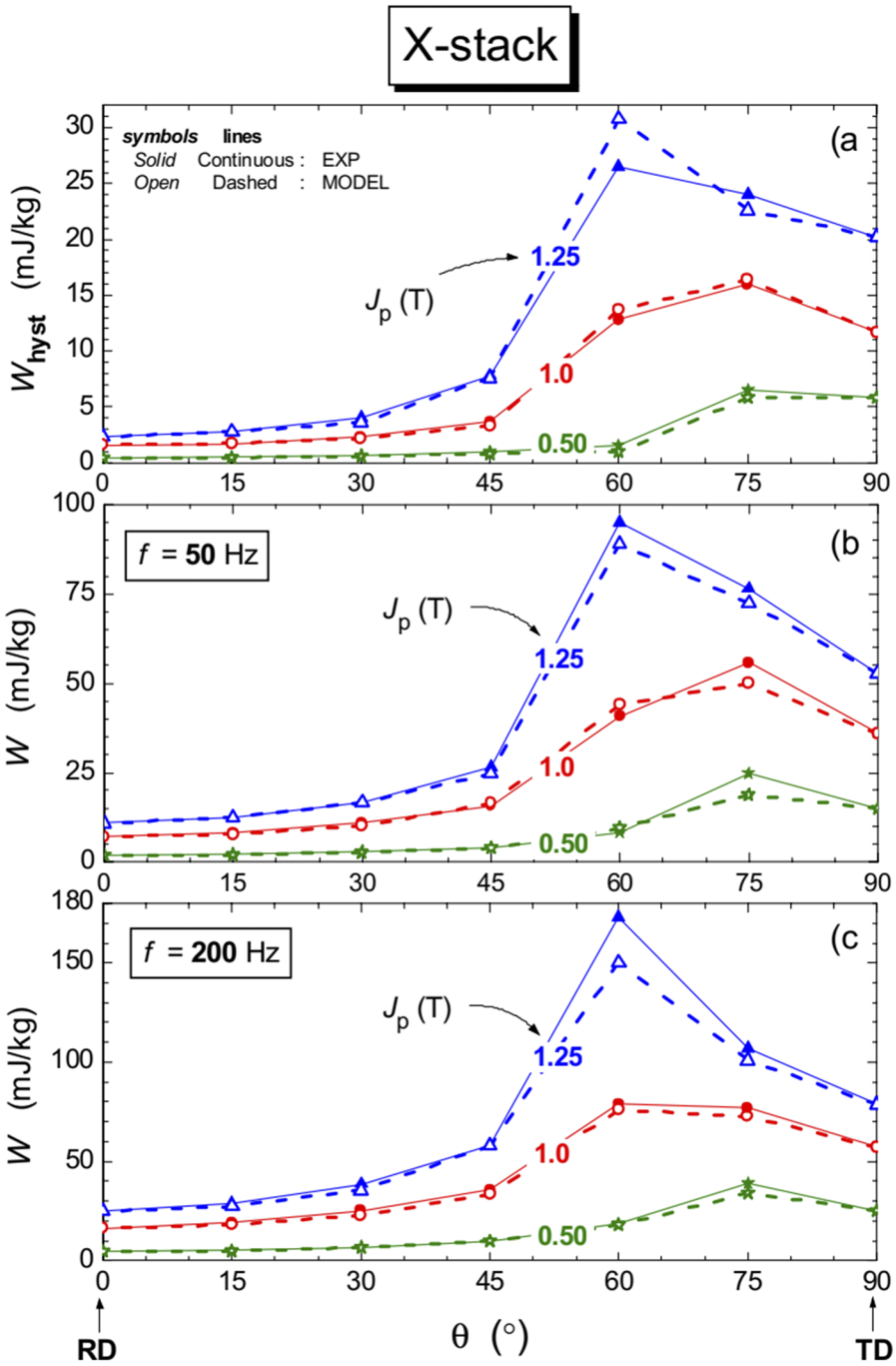

FIG. 13. Same as Fig. 12 for W_{hyst} (a) and the loss measured at 50 (b) and 200 Hz (c) in the X-stacked strips. $W(\theta, f)$ increasingly peaks with increasing f for $\theta = 60°$, an effect chiefly due to the strong distortion of $J_{90}(t)$ [see Fig. 8(a)], in contrast with the sinusoidal behavior of the same quantity in the parallel-stacked strips.

$$W_{\mathrm{exc}}(J_{90,\mathrm{p}}, f) = W_{\mathrm{exc,SIN}}(J_{90,\mathrm{p}}, f) \times \frac{\int_0^T |\mathrm{d}J_{90,\mathrm{p}}/\mathrm{d}t|^n}{J_{90,\mathrm{p}}^n (2\pi f)^{(n-1)} \int_0^{2\pi} |\cos\,\alpha|^n d\alpha}, \quad (13)$$

and, for any θ value,

$$W_{\mathrm{exc}}(J_{\mathrm{p}}, f) = W_{\mathrm{exc}}\left(J_{180,\mathrm{p}}^{(\mathrm{r})}, f\right) + W_{\mathrm{exc}}(J_{90,\mathrm{p}}, f) \quad (14)$$

so that the total loss energy loss $W(J_{\mathrm{p}}, f)$ is always predicted, for any θ value and stacking fashion, as

$$W(J_{\mathrm{p}}, f) = W_{\mathrm{hyst}}(J_{\mathrm{p}}) + W_{\mathrm{class}}(J_{\mathrm{p}}, f) + W_{\mathrm{exc}}(J_{\mathrm{p}}, f), \quad (15)$$

the sum of the components obtained by Eqs. (9), (10), and (14).

The intrinsic response of the GO sheets vs θ, as obtained by strip cross-stacking, can be seen as the result of a somewhat extreme measuring arrangement, while the conventional measurement, performed on either single or parallel-stacked strips, can equally fall into another extreme, as it happens with the Epstein strips, where $J_\perp = 0$. The latter condition, often met in machine cores, strongly diverges with respect to the intrinsic one, as demonstrated by the examples of Figs. 1 and 2, and requires an appropriate interpretative approach. This can be appreciated by comparing the overall behaviors of $W(f)$ vs θ in the parallel- and X-stacked strips shown in Fig. 10. Whatever the case, including intermediate strip arrangements, we can assess these behaviors starting from Eqs. (3) and (4) and, with the support of domain imaging, eventually composing the RD and TD contributions. We can qualitatively understand the $W(f)$ dependence on θ shown in Fig. 10, where both parallel- and X-stacked samples exhibit maximum loss value around $\theta = 60°–75°$, although following quite different trajectories by looking at the involved dw processes. The increase in $W(f)$ starting from $\theta = 0$ (RD) is obviously due to the progressively increasing role of the relatively hard 90° dw transitions. These are necessarily involved in the magnetization process of parallel-stacked strips at any θ value in order to comply with the condition $J_\perp = 0$, while they are not expected to occur for $\theta < 54.7°$ in the X-stacked strips. Here, $W(f)$ is quite low for $\theta < 60°$, but it undergoes a sharp increase at large θ values, where $W(J_{90,\mathrm{p}}, f)$ ([100] [010] phases) largely predominates. We then observe in the example of Fig. 11 how the behaviors of $W_{\mathrm{hyst}}(J_{\mathrm{p}})$ vs θ can be justified as the sum of the calculated contributions $W_{\mathrm{hyst}}\left(J_{180,\mathrm{p}}^{(\mathrm{r})}\right) \cdot \langle v_{180} \rangle$ and $W_{\mathrm{hyst}}(J_{90,\mathrm{p}})$, and we conclude that, by the experimental knowledge of $J_{||}(t)$ and, when existing, of $J_\perp(t)$, the use of Eqs. (7)–(15) leads us, for any experimental J_{p} and θ values, to the complete theoretical description of $W(J_{\mathrm{p}}, \theta, f)$. Figures 12 and 13 summarize the overall comparison of experimental and predicted $W(J_{\mathrm{p}}, \theta, f)$ dependence on θ in the parallel-stacked and X-stacked strips for selected J_{p} and f values. Note the increase in sharpness with increasing f of the $W(\theta, f)$ vs θ curve at high J_{p} values in the X-stacked strips. This effect is understood in terms of correspondingly increased distortion of $J_{90}(t)$ and the related detrimental contribution to W_{class} and W_{exc}, as observed in Fig. 8(a) for $J_{\mathrm{p}} = 1.25$ T and $\theta = 60°$.

IV. CONCLUSIONS

We have discussed and assessed the anisotropic behavior of the magnetization process and energy losses in high-permeability grain-oriented Fe–Si sheets. This is done through the combination of magnetic measurements from 1 to 300 Hz, magneto-optical observations, and physical assumptions regarding the dw processes and their dependence on the cutting angle of the tested strip samples. Such assumptions, supported by the Kerr experiments and relying on the single-crystal approximation, identify the dw processes accounting for the magnetization reversal in the RD and TD strips, respectively, as the building blocks of the magnetization process when the field is applied along any direction. With polarization $J_{||}(t)$ imposed along the field direction, the measurement of the transversal component $J_\perp(t)$ suffices to identify the contributions to the overall magnetization reversal provided by the 180° dw motion inside the [001] phases [$J_{180}(t)$] and by the evolution of the [100] [010] phases (at the expense of the former) by 90° dw transitions [$J_{90}(t)$]. These are exactly the magnetization mechanisms operating along the RD and TD strips, respectively. They occur, for any cutting angle θ to RD, in proportions depending on both θ and degree of flux closure at the sample edges. Full lateral flux closure is obtained by cross-stacking the strips, while the extreme case of large transverse demagnetizing effect is found with parallel-stacked strips (e.g., Epstein samples). Here, $J_\perp(t)$ is always negligible and the problem of finding the two different contributions is easily solved by the sole knowledge of the imposed longitudinal polarization $J_{||}(t)$. The magnetic loss vs frequency and angle θ is then calculated for any given peak polarization value J_{p}, once $J_{180}(t)$ and $J_{90}(t)$ are obtained, by resorting to and combining the corresponding hysteresis, classical, and excess loss components measured with standard methods along RD and TD.

SUPPLEMENTARY MATERIAL

See the supplementary material for a collection of results concerning the magnetization process and the energy losses in the parallel-stacked and X-stacked GO strips. We provide, in particular, (1) Kerr imaging of the domain structure and its evolution along a major quasi-static hysteresis loop for different θ values; (2) energy loss vs frequency behaviors and their comparisons in RD, TD, parallel-stacked, and X-stacked strips for $\theta = 60°$; and (3) comparison of the time dependence of the physical parameters [$J_{90}(t)$, $J_{180}(t)$, $J_{180}{}^{(\mathrm{r})}(t)$, $\nu_{180}(t)$] involved in the magnetization process at 50 Hz in parallel-stacked and X-stacked strips for $\theta = 45°$.

ACKNOWLEDGMENTS

This research work was carried out in the framework of the 19ENG06 HEFMAG project, which was funded by the EMPIR program, and co-financed by the Participating States and the European Union's Horizon 2020 research and innovation program.

AUTHOR DECLARATIONS

Conflict of Interest

The authors have no conflict of interest to disclose.

DATA AVAILABILITY

The data that support the findings of this study are available from the corresponding author upon reasonable request.

REFERENCES

[1]H. Ichou, D. Roger, M. Rossi, T. Belgrand, and R. Lemaître, "Assessment of a grain-oriented wound core transformer for solid state converter," J. Magn. Magn. Mater. **504**, 166658 (2020).

[2]C. Demian, B. Cassoret, J.-F. Brudny, and T. Belgrand, IEEE Trans. Magn. **48**, 1409 (2012).

[3]G. Neidhoefer and A. Schwengeler, "The application and significance of magnetic materials in large generator construction," J. Magn. Magn. Mater. **9**, 112 (1978).

[4]L. Gao, L. Zeng, J. Yang, and R. Pei, "Application of grain-oriented electrical steel used in super-high speed electric machines," AIP Adv. **10**, 015127 (2020).

[5]L. Millan Mirabal, O. Messal, A. Benabou, Y. Le Menach, L. Chevallier, J. Korecki, J.-Y. Roger, and J.-P. Ducreux, "Iron loss modeling of grain oriented electrical steels in FEM simulation environment," IEEE Trans. Magn. (published online 2021).

[6]Y. Matsuo, T. Higuchi, T. Abe, Y. Miyamoto, and M. Ohto, "Characteristics of a novel segment type switched reluctance motor using grain-oriented electric steel," in *2011 International Conference on Electrical Machines and Systems* (IEEE, 2011), pp. 1–4.

[7]Y. Sugawara and K. Akatsu, "Characteristics of a switched reluctance motor using grain-oriented electric steel sheet," in *2013 International Conference on Electrical Machines and Systems (ICEMS)* (IEEE, 2013), pp. 18–23.

[8]J. Ma, J. Li, H. Fang, Z. Li, Z. Liang, Z. Fu, L. Xiao, and R. Qu, "Optimal design of an axial flux switched reluctance motor with grain-oriented electrical steel," IEEE Trans. Ind. Appl. **53**, 5327 (2017).

[9]G. Parent, R. Penin, J. P. Lecointe, J. F. Brudny, and T. Belgrand, "Analysis of the magnetic flux distribution in a new shifted non-segmented grain oriented AC motor magnetic circuit," IEEE Trans. Magn. **49**, 1977 (2013).

[10]M. Birsan and J. A. Szpunar, "Anisotropy of power losses in textured soft magnetic materials," J. Appl. Phys. **80**, 6915 (1996).

[11]H. Wang, C. Li, and T. Zhu, "Hard magnetization direction and its relation with magnetic permeability of highly grain-oriented electrical steel," Int. J. Miner., Metall. Mater. **21**, 1077 (2014).

[12]A. P. S. Baghel, B. Sai Ram, K. Chwastek, L. Daniel, and S. V. Kulkarni, "Hysteresis modeling of GO laminations for arbitrary in-plane directions taking into account the dynamics of orthogonal domain walls," J. Magn. Magn. Mater. **418**, 14 (2016).

[13]K. R. Chwastek, A. P. S. Baghel, M. F. De Campos, S. V. Kulkarni, and J. Szczyglowski, "A description for the anisotropy of magnetic properties of grain-oriented steels," IEEE Trans. Magn. **51**, 1 (2015).

[14]F. Jiang, M. Rossi, and G. Parent, "Anisotropy model for modern grain oriented electrical steel based on orientation distribution function," AIP Adv. **8**, 056104 (2018).

[15]IEC Standard Publication 60404-2, *Methods of Measurement of the Magnetic Properties of Electrical Steel Strip and Sheet by Means of an Epstein Frame*, 3.1 ed. (IEC, 2008).

[16]In the ideal case where the involved magnetic phases have zero coercive field, the circular sample will display an isotropic behavior, as determined by the demagnetizing coefficient.

[17]W. A. Pluta, "Anisotropy of specific total loss components in Goss textured electrical steel," J. Magn. Magn. Mater. **499**, 166270 (2020).

[18]S. Shin, R. Schaefer, and B. C. DeCooman, "Anisotropic magnetic properties and domain structure in Fe-3%Si (110) steel sheet," J. Appl. Phys. **109**, 07A307 (2011).

[19]W. A. Pluta and A. J. Moses, "Prediction of angular variation of specific total loss of Goss oriented electrical steel," Physica B **544**, 28 (2018).

[20]T. Péra, F. Ossart, and T. Waeckerlé, "Numerical representation for anisotropic materials based on coenergy modeling," J. Appl. Phys. **73**, 6784 (1993).

[21]S. Zurek, P. Borowik, and K. Chwastek, "Prediction of anisotropic properties of grain-oriented steels based on magnetic measurements," J. Elect. Eng. **69**, 470 (2018).

[22]F. Fiorillo, L. R. Dupré, C. Appino, and A. M. Rietto, "Comprehensive model of magnetization curve, hysteresis loops and losses in any direction in GO Fe-Si," IEEE Trans. Magn. **38**, 1467 (2002).

[23]A. Hubert and R. Schaefer, *Magnetic Domains* (Springer-Verlag, Berlin, 1998).

[24]L. Néel, "Les lois de l'aimantation et de la subdivision en domains élémentaires d'un monocristal de fer," J. Phys. Radium **5**, 241 (1944).

[25]F. Fiorillo, *Measurement and Characterization of Magnetic Materials* (Academic-Elsevier, San Diego, CA, 2004).

[26]G. Bertotti, "General properties of power losses in soft ferromagnetic materials," IEEE Trans. Magn. **24**, 621 (1988).

[27]E. Barbisio, F. Fiorillo, and C. Ragusa, "Predicting loss in magnetic steels under arbitrary induction waveform and with minor hysteresis loops," IEEE Trans. Magn. **40**, 1810 (2004).

[28]C. Appino, E. Ferrara, F. Fiorillo, C. Ragusa, and O. de la Barrière, "Static and dynamic energy losses along different directions in GO steel sheets," J. Magn. Magn. Mater. **500**, 166281 (2020).